Determination of Gravitational Acceleration through Falling Body and Compound Pendulum Experiments

Student Number: 219036805
Department of Physics, University of Bath, UK, BA2 7AY
Year 2, Semester 2, PH20105

(Dated: May 3, 2023)

Steel ball bearings of varying diameters were dropped into glycerol, a highly viscous fluid. The descent of the ball bearings was captured using slow-motion video recordings, which were subsequently analysed to determine their terminal velocities. These velocities were plotted against the square of the ball bearings' radii, resulting in a linear relationship from which gravitational acceleration, g, was determined to be (9.850 ± 0.0853) ms^{-2}. Additionally, the gravitational acceleration was assessed using a reversible Kater's pendulum by plotting the time periods for different centres of mass. This method yielded a value of (9.801 ± 0.024) ms^{-2}. Both experimental values were compared to the established 9.81137 ms^{-2} for gravitational acceleration, allowing for an evaluation of the effectiveness and accuracy of the two experimental approaches.

I. INTRODUCTION

The fundamental force of gravity underpins humanity's understanding of the cosmos and serves as the bedrock for scientific models of physical reality. Stemming from Newton's law of universal gravitation, gravity is the attractive force that binds together all bodies possessing mass. Despite its seemingly simple nature, gravity plays a critical role in a wide array of phenomena: from the formation of celestial bodies to the more modest motion of Earth-bound objects. To effectively characterise gravity, it is vital to scrutinise two core quantities: the gravitational constant, G, and gravitational acceleration, g.

Gravitational acceleration plays a pivotal role in a variety of practical applications and is a fundamental physical quantity. Its significance is evident in fields such as geophysics, engineering, and aerospace technology: precise knowledge of g is crucial for satellite orbit calculations, geodetic surveys, and aircraft navigation systems. Moreover, it is indispensable in the design and analysis of structures, vehicles, and machinery consistently exposed to gravitational forces [1].

The gravitational constant, initially introduced in the aforementioned Newton's law, quantifies the strength of the gravitational force between two objects. The law posits that the attractive force exerted on their masses, m_1 and m_2, separated by a distance r, is given by

$$F = G\frac{m_1 m_2}{r^2}. \tag{1}$$

In a system consisting of more than two masses, each mass will experience the net gravitational pull of the bodies surrounding it, in the direction of the system's centre of mass. Previously, the gravitational constant has been determined through a myriad of methods, including the pioneering Cavendish experiment: the first to successfully derive an accurate value for G. Henry Cavendish's value of 6.74×10^{-11} Nm^{2}kg^{-2} [2] differs only 1% from the currently accepted CODATA statistic of 6.67408×10^{-11} Nm^{2}kg^{-2} [3].

When considering a mass m located near the Earth's surface, equating Newton's second law to the gravitational force yields a formula for gravitational acceleration,

$$g = G\frac{M_\oplus}{R_\oplus^2}, \tag{2}$$

with $M_\oplus$ representing the mass of the Earth and $R_\oplus$ denoting its radius. This correlation between g and G is essential for understanding the behaviour of objects under the influence of gravity.

Owing to the Earth's oblate spheroidal shape and internal density variations, gravitational acceleration is not uniform across the planet's surface. As altitude rises, g typically diminishes due to the increasing distance from Earth's centre. Moreover, g varies with latitude, being larger near the poles and smaller near the equator. This fluctuation of gravitational acceleration is due to the Earth's equatorial bulge, a direct consequence of the centrifugal force that emerges from the planet's rotation [4].

This study seeks to determine an accurate value for g by conducting experiments involving falling bodies and compound pendulums. The falling body experiment considers both the motion of objects in free-fall and the effect of fluid viscosity, which leads to viscous drag forces that can be modelled in distinct flow regimes. For instance, in the laminar flow regime, the drag force can be modelled using Stokes' Law,

$$F_D = 6\pi\mu r v, \tag{3}$$

where μ is the dynamic viscosity of the fluid, r is the radius of the ball, and v is the relative velocity of the ball and the fluid. Conversely, in the turbulent flow regime, the drag force is given by

$$F_D = \frac{1}{2}C_D\rho A v^2, \tag{4}$$

where C_D denotes the drag coefficient, ρ signifies the fluid density, and A refers to the cross-sectional area. In fluid mechanics, the flow regime is predicted using Reynold's number, which is the ratio of inertial forces to viscous forces in a fluid experiencing internal relative motion due to varying fluid velocities,

$$R_e = \frac{F_{inertial}}{F_{viscous}} = \frac{2\rho v r}{\mu}. \tag{5}$$

A value of $R_e < 1$ indicates laminar flow, whilst $1000 < R_e < 2\times10^5$ indicates a turbulent flow. In between these ranges lies transitional flow, hence the name, which has no clear, single model but consists of several approximations for separate ranges of R_e [5].

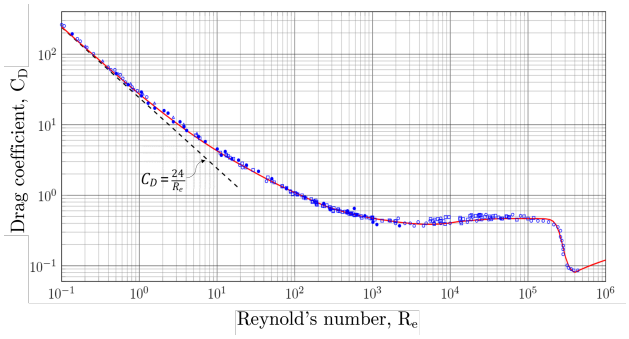

FIG. 1. [6] Drag coefficient of a smooth sphere as a function of Reynold's number. There is a linear relationship between the drag coefficient and Reynold's number for values of $R_e < 1$. Substituting this value for C_D into equation 4 produces Stokes' Law in Equation 3.

Simultaneously, the experiment with pendulums investigates the oscillatory motion of rigid bodies, a topic that has been studied since the work of Christiaan Huygens in the 17$^{\text{th}}$ century. The simple pendulum, both in the small angle approximation and for arbitrary angles, serves as the foundation for understanding the motion of a compound pendulum. For small angles, the time period of a simple pendulum is reduced to

$$T = 2\pi\sqrt{\frac{l}{g}}, \tag{6}$$

where l represents the pendulum's length. In contrast, for a non-linear pendulum that deviates from the small angle approximation, the time period can be defined as

$$T = 4\sqrt{\frac{l}{g}}K(k), \tag{7}$$

in which $K(k)$ is a complete elliptic integral of the first kind and k is the elliptic modulus, with a range of $0 \leq k^2 \leq 1$. When dealing with compound pendulums, a straightforward modification can be applied:

$$l = \frac{I_0}{Md}, \tag{8}$$

where I_0 stands for the moment of inertia about the point of rotation, M is the total mass of the pendulum, and d refers to the distance from the centre of mass to the point about which the pendulum is rotating [7].

In this report, we present a comprehensive approach to determining gravitational acceleration through experiments on falling bodies and compound pendulums, with a focus on Kater's pendulum. By examining the motion of free-falling objects and the effects of fluid viscosity, as well as the oscillatory motion of rigid bodies, we aim to contribute to a deeper understanding of gravity and its applications in various fields. Furthermore, our research offers valuable insights into the precision and limitations of these methods, guiding future research and enhancing our knowledge of gravitational phenomena.

II. EXPERIMENTAL

A. Free-Fall

Multiple steel ball bearings ranging from roughly 2-20 mm in diameter were chosen for this experiment. Their mass and radius were recorded with a balance and a digital caliper. An electromagnet holding these balls was secured above a transparent cylindrical tube with equally spaced markings down its surface. It was approximately 40-50 cm tall and 6-7 cm in diameter: large enough to significantly reduce boundary-induced drag between the ball and tube.

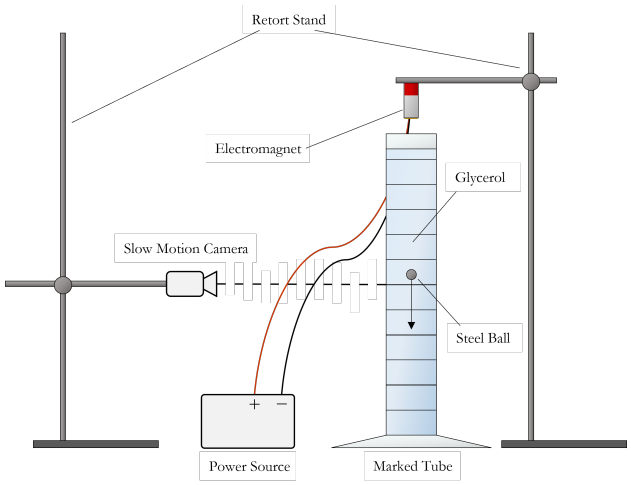

FIG. 2. When the power source is turned off, the connected electromagnet releases the ball bearing. As the sphere descends it is recorded by a slow motion camera at 240.37 fps. This camera is aligned with a marking on the tube that was previously determined as a point at which terminal velocity had been reached.

The tube was filled nearly to the top with glycerol, and the equipment was carefully arranged. A stopwatch was utilized to measure the time it took for each ball to travel from distinct markings on the tube to the bottom.

The velocity was monitored, and once it remained consistent across consecutive trials, the camera was adjusted to focus on the relevant marking. This adjustment aimed to minimize parallax errors during the analysis. Due to the absence of a synchronized dual-camera setup, which would have further mitigated parallax errors, the timer was stopped when the ball came to a complete halt at the tube's bottom.

B. Kater's Pendulum

Firstly, the knife-edges were confirmed to not be dull and then the distance between them was measured using a metre rule. Being dull would make the effective point of rotation below where the knife-edge meets the supporting block and as such the effective length, L_{eff}, between knife-edges would not be accurately measured.

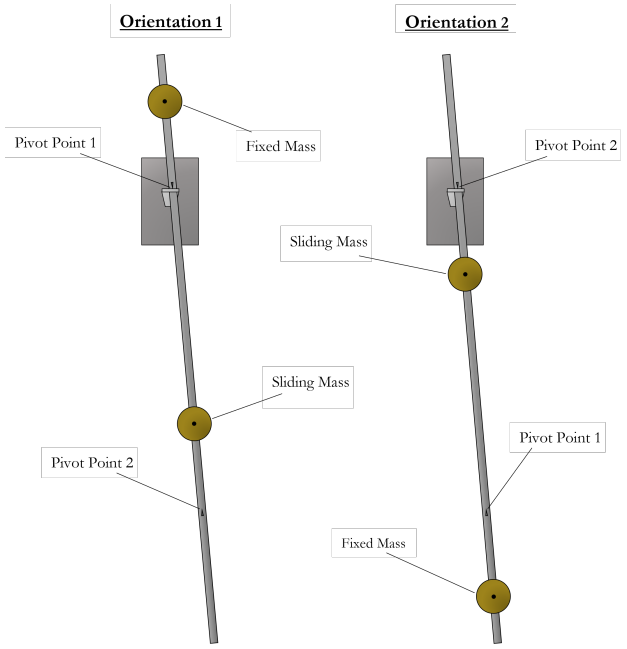

FIG. 3. The pendulum consists of two opposing knife edges, a fixed mass, and a sliding mass. The sliding mass' position can be adjusted between the two pivots, in turn changing the centre of mass and therefore the time period of the pendulum. In addition to the centre of mass, the position of the fixed mass affects the total inertia when the pendulum is reversed, altering the rate of change of the time period. This creates the intersections shown in Figure 5.

The pendulum was hung from a knife-edge, passing through a light gate positioned beneath. The gate recorded the number of oscillations while a stopwatch was used to time 50 of these oscillations. Aligned with the left side of the pendulum, lines of 5 cm increments were marked on masking tape stuck to the wall behind. A straight wooden stick was pressed flat against the wall to hold the pendulum in position before releasing and starting the timer. The sliding mass was moved between the two pivots, its position marked out. The radius of the sliding mass was measured in order to mark where the edge should be placed for its centre of mass to be a specified distance from the pivot of rotation.

III. RESULTS AND SPECIFIC DISCUSSION

A. Steel Ball in Free-Fall

The initial experiment's primary goal was to ascertain a value for gravitational acceleration by observing the velocities of falling ball bearings in air while accounting for drag. Unfortunately, the low viscosity of air combined with the limited technology at hand rendered this task unachievable. The analysis began with the equation of motion for a freely falling object,

$$m\frac{dv}{dt} = mg - kv^2, \tag{9}$$

where m denotes the mass of the ball, k is a constant representing drag, and v is the velocity. Given that acceleration is zero at terminal velocity, an equation for velocity as a function of time can be derived:

$$v = v_T \tanh\left(\frac{gt}{v_T}\right). \tag{10}$$

The essential challenge in this case was the unknown terminal velocity of the ball bearings, which, as a function of g, could not be calculated. Consequently, v_T would need to be determined experimentally. However, due to insufficient space and a lack of necessary equipment, this could not be accomplished.

Investigating the possibility of conducting the experiment in a highly viscous fluid, where a measurable terminal velocity could be achieved, the chosen fluid was glycerol—a compound with a viscosity approximately 1500 times greater than water. Nonetheless, a significant factor not applicable in air, namely buoyancy due to fluid displacement, had to be considered. While buoyancy was negligible in air due to its extremely low density, the high density of glycerol made it impossible to disregard. Furthermore, it was necessary to re-evaluate the Reynolds number for the ball bearings in this new context.

Table I demonstrates that the first six balls experienced laminar flow while falling in glycerol; however, a deliberate decision was made to exclude the sixth ball when constructing the linear square regression. As illustrated in Figure 1, the relationship between drag and Reynolds number is not perfectly linear as R_e approaches 1, which would yield a less accurate value for g.

The updated equation of motion accounted for the upthrust due to glycerol and utilized Stokes' Law, Equation 3, as the model for drag:

$$m\frac{dv}{dt} = \frac{4}{3}\pi R^3(\rho_{steel} - \rho_{glycerol})g - 6\pi\mu Rv. \tag{11}$$

TABLE I. Table displaying the diameters of the ball bearings used and their Reynold's numbers at terminal velocity

Diameter (mm)	Reynold's Number
1.80	0.0205
2.80	0.0609
3.80	0.1426
4.80	0.2688
5.80	0.4640
6.80	0.7123
7.80	1.0214
8.80	1.4081
9.80	1.8776
11.80	2.9624
17.80	7.1996

Here, R represents the radii of the balls and ρ denotes density. The following equation, in terms of terminal velocity, could then be derived:

$$v_T = \frac{2}{9}\frac{\rho_{steel} - \rho_{glycerol}}{\mu} g R^2. \tag{12}$$

Initially, the balls were recorded at 240.37 fps, which was later reduced to 30 fps before being exported to a video editor capable of examining individual frames. After collecting the time taken for each ball to fall through a series of markings on the measuring cylinder, their terminal velocities were calculated and plotted against the square of their radii.

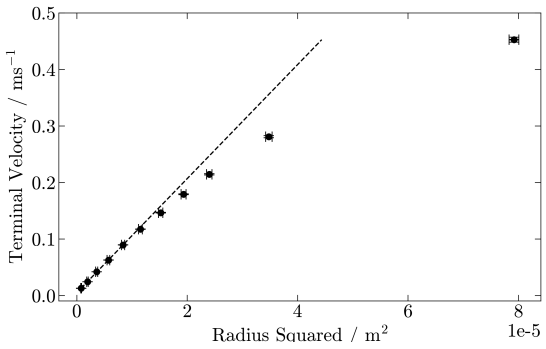

FIG. 4. A graph illustrating the relationship between the terminal velocity of the ball bearings and their radii is presented. As the conditions fall well within the range of laminar flow, the graph initially displays a linear trend before transitioning into a polynomial shape, which aligns with the predicted calculations of the Reynolds number.

This graph has a slope of (10088.67 ± 84.62) m^{-1}s^{-1} giving a value of (9.850 ± 0.0853) ms^{-2} for gravitational acceleration. The true value can be calculated using the International Gravity Formula (1980) which accounts for latitude and the Free Air Correction which depends on height above sea level. The experiment took place at a latitude of 51.3787° and 181 m above sea level.

$$\text{IGF} = 9.780327(1 + 0.0053024\sin^2\phi - 0.0000058\sin^2 2\phi)$$

$$\text{FAC} = -3.086 \times 10^{-6} \times h$$

$$g = \text{IGF} + \text{FAC}$$

In this, ϕ is the latitude and h is the height above sea level [4]. Implementing this formula gives a theoretical local value for g as 9.81137 ms^{-2}. This falls within the error given from the free-fall experiment, and the value for gravitational acceleration determined differs by 0.394%.

B. Kater's Pendulum

The non-linear framework serves as an excellent starting point before transitioning to the linear model. Beginning with the equation for torque,

$$\tau = -Mgd\sin\theta = I_0\ddot{\theta}, \tag{13}$$

where $\ddot{\theta}$ denotes the angular acceleration. By rewriting this as a second-order, homogeneous differential equation, the equation below is obtained:

$$\ddot{\theta} + \frac{Mgd}{I_0}\sin\theta = 0. \tag{14}$$

The solution to this differential equation is not elementary and is expressed in terms of Jacobi Elliptic Functions:

$$\theta(t) = 2\arcsin\left(k \cdot cd\left(t\sqrt{\frac{Mgd}{I_0}}, k\right)\right), \tag{15}$$

where t is the time and $k = \sin\frac{\theta_0}{2}$, with θ_0 being the initial angle. Leveraging the understanding that the change in kinetic energy is equal to the change in gravitational potential, the angular velocity can be established as

$$\frac{d\theta}{dt} = \sqrt{\frac{2Mgd}{I_0}(\cos(\theta) - \cos(\theta_0))}. \tag{16}$$

Integrating its reciprocal to determine the time period results in

$$T = 4\sqrt{\frac{I_0}{2Mgd}}\int_0^{\theta_0}\frac{d\theta}{\sqrt{\cos(\theta) - \cos(\theta_0)}}. \tag{17}$$

This can be expressed in terms of elliptic integrals:

$$T = 4\sqrt{\frac{I_0}{Mgd}}K(k). \tag{18}$$

Here, $K(k)$ is a complete elliptic integral of the first kind, defined by

$$K(k) = F(\frac{\pi}{2}, k) = \int_0^{\frac{\pi}{2}}\frac{du}{\sqrt{1 - k^2\sin^2(u)}}. \tag{19}$$

From the parallel axis theorem, the moment of inertia of an object about an axis parallel to one through its centre of mass is related to the moment of inertia about that centre of mass, I_c, by:

$$I_0 = I_c + MR^2, \tag{20}$$

where R is the distance between the two axes. In this case, the axis of I_0 and I_c. Substituting the equation for I_0 into Equation 18,

$$T_1 = 4\sqrt{\frac{I_c + Ml_1^2}{Mgl_1}}K(k) \tag{21}$$

$$T_2 = 4\sqrt{\frac{I_c + Ml_2^2}{Mgl_2}}K(k) \tag{22}$$

where l_1 and l_2 are the distances between each respective pivot point and the centre of mass. If the weights on the pendulum are adjusted such that $T_1 = T_2$, then the central inertia simplifies to

$$I_c = Ml_1l_2. \tag{23}$$

Provided l_1 differs significantly from l_2, that is, the pendulum is quite asymmetric. Substituting the equation for I_c at equal time periods into Equation 21 or 22,

$$T = 4\sqrt{\frac{l_1 + l_2}{g}}K(k) = 4\sqrt{\frac{L}{g}}K(k), \tag{24}$$

where L is the distance between the two pivots.

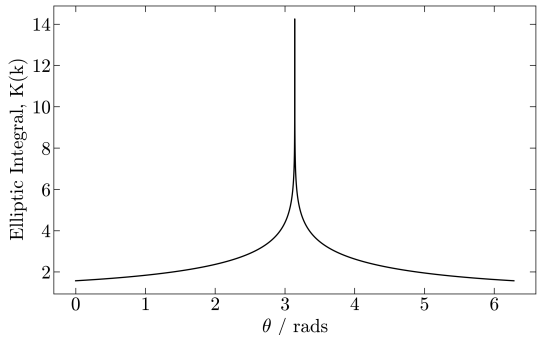

FIG. 5. This figure demonstrates the complete elliptic integral of the first kind as a function of the initial angle. As can be seen, for small angles, $K(k) \to \frac{\pi}{2}$ and for large angles close to π rads, $K(k) \to \infty$. This makes sense, a vertically upwards pointing pendulum with no initial horizontal velocity component would essentially have an infinite time period as it would not swing either way. Furthermore, angles close to it would take a significant time to start moving rapidly under the effect of gravity.

As Figure 5 demonstrates, in the small angle approximation Equation 24 reduces to,

$$T = 2\pi\sqrt{\frac{L}{g}}. \tag{25}$$

Moreover, utilising the knowledge that $\sin\theta = \theta$ for small angles and that as $k \to 0$, $cd(x, k) = \cos x$, Equation 15 becomes

$$\lim_{\theta_0 \to 0}[\theta(t)] = 2\arcsin\left(\frac{\theta_0}{2} \cdot \cos\left(t\sqrt{\frac{Mgd}{I_0}}\right)\right), \tag{26}$$

which rearranges to:

$$\theta(t) = \theta_0 \cos\left(t\sqrt{\frac{Mgd}{I_0}}\right). \tag{27}$$

This solution is confirmed when solving Equation 14, substituting $\sin\theta$ for θ.

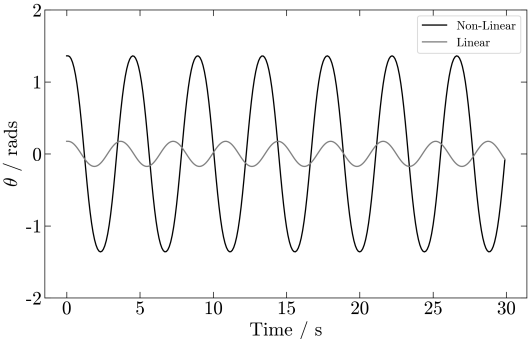

FIG. 6. A graph of angular displacement as a function of time. The figure shows that, for angles in the non-linear model, there is an increased time period dependent on the initial angle. All initial angles within the small angle approximation have the same time period.

Starting with Kater's pendulum in the linear model, the data was plotted in Figure 7.

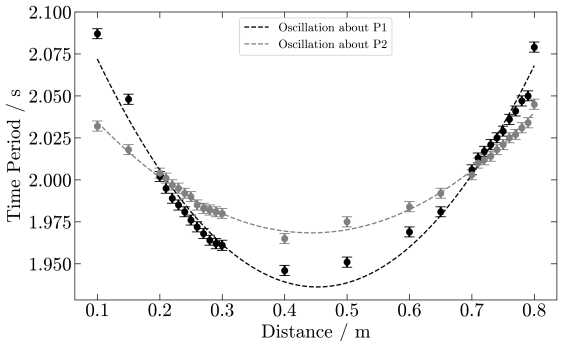

FIG. 7. This figure depicts the time period of the pendulum against the distance from the sliding mass to the knife-edge about which the pendulum was oscillating. The initial angle was 11° and each measurement of the time period was iterated three times.

The intersects were found to be at $(0.216 \pm 0.048\text{ m}, 1.997 \pm 0.048\text{ s})$ and $(0.710 \pm 0.150\text{ m}, 2.008 \pm$

0.237 s) which gave a value of 2.003 ± 0.121 s for the time period. This, in turn, achieved a quantity of (9.802 ± 1.184) ms^{-2} for gravitational acceleration. This large error is due to the data points that stray quite a fair distance from the fitted curve in the middle. Although the value determined only differs 0.097% from the true value of 9.81137 ms^{-2}.

In order to reduce this error a new approach was decided upon. Utilising the equation derived by Friedrich Bessel in 1826, as long as the periods measured from each pivot, T_1 and T_2, are close in value,

$$T^2 = \frac{T_1^2 + T_2^2}{2} + \frac{T_1^2 - T_2^2}{2}\left(\frac{l_1^2 - l_2^2}{l_1^2 + l_2^2}\right). \tag{28}$$

The value of g was found to be (9.801 ± 0.024) ms^{-2}. This still has a small percentage difference to the established value, only 0.106% but a much less significant margin of error that still encloses 9.81137 ms^{-2}.

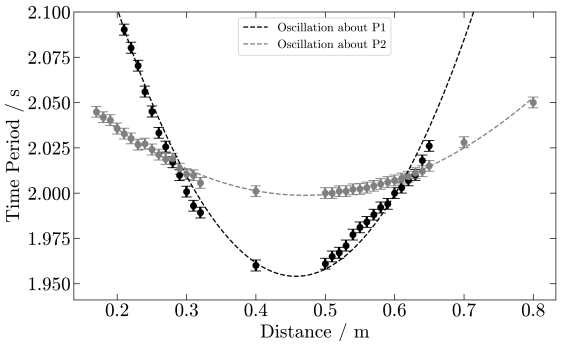

FIG. 8. This figure illustrates the relationship between the period of the pendulum and the distance from the sliding mass to the pivot point. The initial angle of oscillation was set at 27 degrees and as such the data is a result of non-linear motion.

For large angles, this data was not useful, the value ascertained for g was (11.078 ± 0.031) ms^{-2} after employing Equation 28. This substantial difference to the true value will be reviewed in the general discussion.

IV. GENERAL DISCUSSION

For the free-fall experiment, the use of slow-motion recording was a valuable tool in capturing the motion of the ball. However, various factors, such as bubbles in the glycerol, difficulties in determining the exact point of contact between the ball and the bottom, and increased drag near the floor surface, introduced errors in the measurements. To enhance the accuracy and reliability of this experiment in the future, suggested improvements include removing bubbles from the glycerol (perhaps through heat), employing a wider and longer tube, and using a dual-camera system to minimize parallax error.

In Kater's pendulum experiment, the theoretical model predicted minimal errors. However, the inaccuracies in the data collection, mostly at the troughs of the curves, led to significant deviations from the expected results. More data points and smaller steps would be advantageous in future trials.

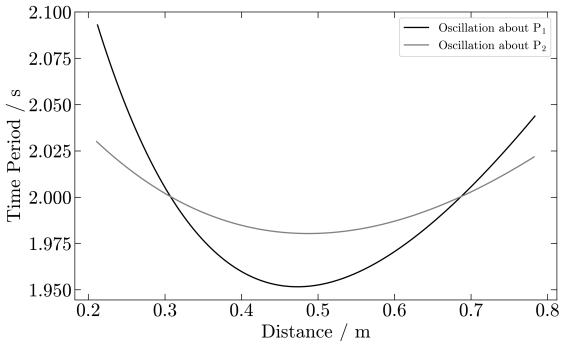

FIG. 9. This graph serves as a model for all initial angles within the small angle approximation. The time period is depicted in relation to the distance from the sliding mass to the point about which the pendulum is oscillating.

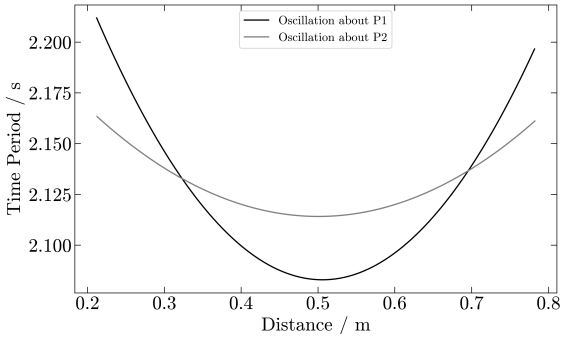

FIG. 10. This graph demonstrates the time period of the pendulum as a function of the sliding mass' distance from the pivot point. As can be seen, the time period is dependent on the initial angle for pendulums outside of the small angle approximation, thereby increasing the time period at which the two orientations intersect.

The results from both experiments, represented in Figures 9 and 10, were compared to Figures 7 and 8. The discrepancies between the graphs can be primarily attributed to approximations made for the moment of inertia and unaccounted drag. By incorporating drag into the pendulum's equation of motion,

$$\ddot{\theta} = -\frac{Mgd}{I_0}\sin\theta - b \cdot \dot{\theta}|\dot{\theta}|, \tag{29}$$

a more accurate representation of the pendulum's behavior can be obtained.

For Figure 11, the drag coefficient, b, had a value of 0.0256 ± 0.0006. This method of analysing the drag can

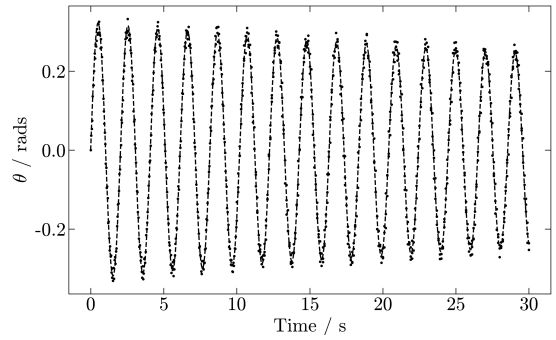

FIG. 11. The Blender programme tracked the amplitude of the sliding mass as the pendulum swung producing a graph of the angle of deviation against time. This was done for small angle oscillations and a curve was fitted by solving Equation 29 in Python.

be used to refine future experiments, especially for large angles where the time period decay was more significant due to increased velocity, resulting in a reduced average.

V. CONCLUSION

In conclusion, the experiments conducted to determine the gravitational acceleration, g, have demonstrated the importance of careful consideration of experimental factors, such as drag and other sources of error. The free-fall experiment highlighted the need to eliminate any sources of error possible. For Kater's pendulum, although accurate determination of g was achieved, further refinements could be made by acquiring more data points and improving the theoretical model by accounting for drag.

This study provides a solid foundation for future investigations into the behavior of objects under the influence of gravity. The improved experimental setups can be utilized in more comprehensive studies on drag forces and their impact on the motion of free-falling objects and pendulums. Moreover, the development of a more accurate theoretical model accounting for drag and other sources of error will benefit future research in areas such as fluid mechanics and aerodynamics.

Further exploration of non-linear pendulum motion requires refining of the experiment to account for drag during data collection, although it may be more practical to focus on small angle approximations due to the complexity of non-linear motion. Application of these improved experimental methods and theoretical models to other fields, such as engineering and materials science, may provide valuable insights into the design and optimization of structures and materials under various gravitational conditions. Overall, the findings of this study offer a stepping stone for further advancements in the understanding of gravitational effects on motion and their applications in diverse scientific disciplines.

In terms of determining an accurate value for gravitational acceleration, pendulums offer a more precise value than free-fall and a significantly smaller source of error.

VI. MY ROLE ON THE PROJECT

Throughout the project, my primary responsibilities centered on both computational and theoretical aspects. I lead the development of the theoretical foundation for the free-fall and Kater's pendulum experiments. In addition, I provided guidance in designing and planning the free-fall experiment.

Alongside these responsibilities, I created all the figures featured in this report, with the exception of the drag coefficient against Reynold's number graph, which was sourced from an online resource. Furthermore, I conducted error analysis by calculating the propagation of errors for each experiment. This process allowed us to gain a better understanding of the sources of uncertainty and devise necessary improvements for future iterations of the experiments.

Overall, my contributions to the project spanned a variety of computational and theoretical tasks, ensuring a comprehensive grasp of the underlying physics and offering a strong foundation for data analysis and interpretation. The Python code for the graphs can be found on Github at https://github.com/lewisjd/Gravitational-Acceleration.

VII. REFERENCES

[1] BOOK: G. Tipler, P. A. & Mosca. Physics for Scientists and Engineers with Modern Physics. W.H. Freeman and Company, New York, 6th edition, 2007.
[2] ARTICLE: Henry Cavendish. Experiments to determine the density of the earth. 1798, 88, p469–526.
[3] WWW: J. L. Lee. Gravitational Constant G https://www.nist.gov/news-events/news/2016/11/big-g-redux-solving-mystery-perplexing-result.
[4] BOOK: W. Torge. Geodesy. Walter de Gruyter, Berlin, 3rd edition, 2001.
[5] BOOK: F. M. White. Fluid Mechanics. McGraw-Hill Education, New York, 8th edition, 2016.
[6] WWW: K. Dusling. Drag Coefficient of a Smooth Sphere https://kdusling.github.io/teaching/Applied-Fluids/ImageDisplay.html?src=DragSphere.
[7] BOOK: H. D. Young. Fundamentals of Mechanics and Heat. McGraw-Hill, New York, 1st edition, 1964.